communications physics

ARTICLE

https://doi.org/10.1038/s42005-023-01489-2 OPEN

Photonic integrated processor for structured light detection and distinction

Johannes Bütow [1,2], Varun Sharma[1,3], Dorian Brandmüller [1], Jörg S. Eismann[1,2,4,5] & Peter Banzer [1,2,3,4,5]✉

Integrated photonic devices are pivotal elements across research fields that involve light-based applications. Particularly versatile platforms are programmable photonic integrated processors, which are employed in applications like communication or photonic computing. Free-space distributions of light can be coupled to such processors, which subsequently control the coupled light on-chip within meshes of programmable optical gates. This enables access to the spatial properties of free-space light, particularly its relative phase, which is usually challenging to measure. Here, we discuss and show the detection of amplitude and phase distributions of structured higher-order light beams using a multipurpose photonic processor. This can be used to directly distinguish light's orbital angular momentum without including additional elements interacting with the free-space light. We envision applications in a range of fields that rely on the spatial distributions of light's properties, such as microscopy or communications.

[1] Institute of Physics, University of Graz, NAWI Graz, Universitätsplatz 5, 8010 Graz, Austria. [2] Christian Doppler Laboratory for Structured Matter Based Sensing, Institute of Physics, Universitätsplatz 5, 8010 Graz, Austria. [3] Max Planck-University of Ottawa Centre for Extreme and Quantum Photonics, 25 Templeton St., Ottawa, Ontario K1N 6N5, Canada. [4] Max Planck Institute for the Science of Light, Staudtstr. 2, 91058 Erlangen, Germany. [5] Institute of Optics, Information and Photonics, University Erlangen-Nuremberg, Staudtstr. 7/B2, 91058 Erlangen, Germany. ✉email: peter.banzer@uni-graz.at

The small-footprint integration of optical and photonic components allows for on-chip processing via controlled routing, interaction, and manipulation of light. Such photonic integrated circuits have paved the pathway towards the development of novel devices across various research areas[1]. More recently, actively controlled reconfigurable photonic integrated circuits have emerged and are being explored experimentally[2–4]. These chips process waveguide modes inside a reprogrammable light processing unit with the help of meshes of optical gates / Mach-Zehnder interferometers and thus losslessly manipulate relative on-chip amplitudes and phases across the photonic circuit. Tailoring, rerouting and assessing on-chip light in such interferometric meshes has enabled applications across various fields, like communication[5], information processing and quantum optics[6,7] and photonic computing and neural networks[8–10]. Programmable photonic processors like these can also be interfaced to free-space, e.g., via grating coupler based layouts. Operating where on-chip waveguide modes meet off-chip free-space light, the resulting photonic chips can be utilized in different ways and used for multiple purposes in free-space optics[11,12]. This can, for example, allow the targeted generation of structured light[13], the measurement of amplitude and phase[14,15], the separation of arbitrary modes[16] or the coherent self-control of free-space modes[17].

Such a free-space interface intricately connects these devices to distributions of free-space modes and their natural next application is the measurement and distinction of higher-order light beams that feature intricate amplitude and phase distributions. Such beams are facilitated in advanced applications like microscopy, communication or quantum entanglement[18–22]. However, intensity-only measurements are usually blind to phase or polarization of such beams, although information is usually encoded in these parameters. For their characterization, more elaborate approaches are required. For example, identifying the helical phase-front of a Laguerre-Gaussian beam and the related property of orbital angular momentum[23] requires phase sensitive spatially or angularly resolved measurements, which can be experimentally challenging. Consequently, considerable research has been focusing on the convenient identification of such beams with orbital angular momentum[24] using interferometry, Shack-Hartmann wavefront sensors, spatial light modulators[25,26], convolutional neural network based approaches[27] or specifically designed integrated components[28,29].

Here, we advance the utilization of photonic integrated processors to spatially resolve amplitude and phase of light, recently reported in Ref. [15], with a focus on applications involving structured light. We discuss and demonstrate the detection and distinction of structured higher-order light beams, including but not limited to Laguerre-Gaussian modes. We specifically show how such a device, even with only 16 pixels, can distinguish a wide range of beams, e.g., Laguerre-Gaussian modes carrying orbital angular momentum. This is a next step towards an all-integrated, versatile and high-resolution platform for the measurement and control of amplitude and phase distributions of such beams, going far beyond information and functionality offered by a conventional camera. The results presented in this article extend the range of applications of multipurpose photonic processors, highlighting their strength in terms of controlling on-chip light for free-space applications.

Results

On-chip processing of light. A die shot of the photonic integrated processor used in this work is shown in Fig. 1a. The utilized processor is composed of three major sections, each including multiple integrated components: (1) A central light processing unit comprised of a mesh of reconfigurable Mach-Zehnder interferometers (universal 2×2 optical gates), highlighted in yellow and also shown schematically in Fig. 1b. (2) A free-space interface connected to the mesh via single-mode waveguides, highlighted in blue, and (3) a monitoring interface, highlighted in red. The free-space and monitoring interface are composed of carefully arranged grating couplers terminating the individual waveguides. These grating couplers can either act as emitters to free space or they can be used to couple free-space light into the waveguides, sampling impinging light beams comparable to the pixels of a normal camera. Beyond the capabilities of conventional pixels, however, the phase information of the sampled light is preserved in the coupled waveguide modes that now travel across the chip. This is essential for the measurement of structured free-space light discussed in this manuscript. In reverse, when grating couplers couple out on-chip light into free space, the emitted light has the same relative intensities and phases as the terminated waveguide modes. Grating couplers can thus be utilized for off-chip power monitoring of waveguide modes transmitted through the interferometric mesh by means of imaging or fiber coupling via the monitoring interface (red).

Fundamental to the photonic integrated processor is its interface to free space on the left (blue) which is used to sample free-space light distributions. This interface can feature any layout of grating couplers, e.g., a regular grid-like layout similar to pixels of a normal camera. However, our prototype device is restricted to 16 grating couplers and has thus been carefully designed to enable multiple applications. The chosen arrangement along two concentric rings is, for example, well suited for applications featuring rotational symmetry. Details on this ring-like layout are discussed in more detail in the method section. The final crucial aspect of the photonic integrated processor is how on-chip light is processed in the interferometric mesh which acts as a central light processing unit, see Fig. 1b. Mach-Zehnder interferometers (yellow) arranged in a binary-tree can reroute the flow of light across the chip. On-chip amplitudes and phases can be accurately controlled across the interferometric mesh. Light coupled into the circuit via the free-space interface and traveling through the mesh can, for example, be processed to be fully or partially combined in a single output waveguide thus enabling sorting, merging or adapting to free-space modes. Alternatively, by running light backward through the programmed mesh, this platform can also be used for other purposes. Modes of arbitrary relative intensity and phase could be generated in the circuit and emitted into free-space to form tailored distributions of structured light[13], similar to optical phased arrays or beam shapers[30,31]. Note, that while the central light processing unit does not introduce any fundamental loss[14], the manufactured on-chip components are not perfect, and, e.g., waveguide side-wall roughness is introducing transmission losses. However, these are smaller than 2 dB over the whole photonic circuit and their impact can be further mitigated by routing the waveguides such that they share the same geometrical lengths. This can be seen in Fig. 1a between the free-space interface and the central light processing unit. Remaining losses are thus balanced and do not affect the measured relative amplitudes.

Before we describe how the photonic processor was used experimentally to measure higher-order beams we briefly discuss the utilization of the interferometric mesh. All mentioned applications rely on processing light in the central light processing unit while monitoring resulting waveguide intensities. One approach to measure unknown amplitude and phase distributions is based on self-alignment and power minimizations[11,14], after training the device with specifically designed input distributions of light. Tracking/configuration times of interferometric meshes operated this way can be sub-

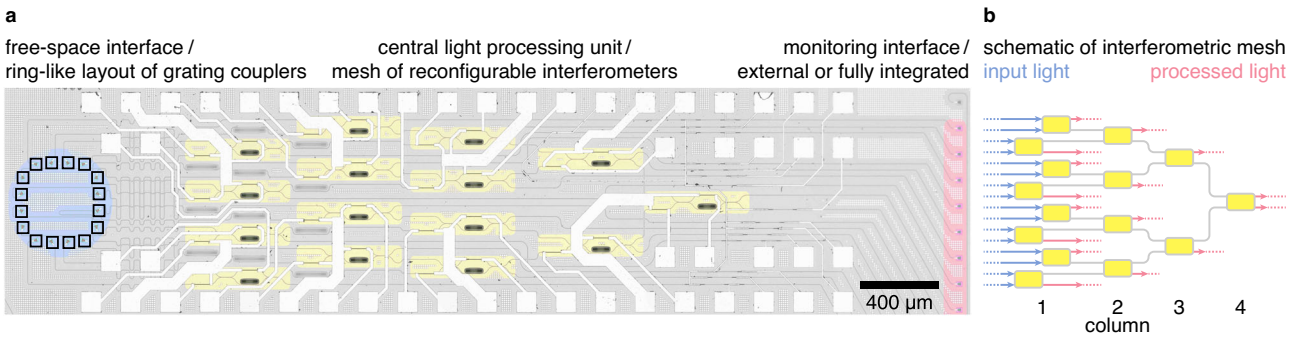

Fig. 1 Utilized photonic integrated processor. a Optical microscope image. On-chip light flows from left-to-right and is processed losslessly in a central mesh of reconfigurable Mach-Zehnder interferometers (yellow). **b** Schematic view of the central light processing unit's waveguide and interferometer layout.

millisecond, enabling fast operation and self-stabilization[5,16]. However, the specific training distributions require prior generation, and it can be challenging and demand elaborate setups to accurately send them onto the free-space interface. A second approach, described in detail in Ref. [15], relies on calibrating the interferometric mesh with a single reference input beam thereby characterizing all on-chip components simultaneously. This reveals the full transmission matrix of the mesh, which can be utilized in subsequent applications to configure the mesh as required. On-chip waveguide modes can now be examined by monitoring the effect the interferometric mesh has on the transmitted intensities upon processing. The photonic system, utilized this way, can handle imperfect components like non 50:50 on-chip beam splitters, and no further training of the device is required. Here we follow the second approach and further details on the principle of operation of the photonic integrated processor are discussed in the method section. We calibrate the mesh with a circularly polarized Gaussian beam of sufficient diameter (2 mm) to act as amplitude and phase reference. Unknown free-space distributions of light can afterwards be analyzed with regard to their relative amplitudes and phases at the grating coupler positions of the free-space interface.

Measuring higher-order beams. An illustration of the setups core components is shown in Fig. 2a. A free-space laser beam with a wavelength of 1570 nm is converted into a scalar spatial mode of light using a reflective phase-only spatial light modulator. The resulting higher-order beam is polarized circularly before finally passing a lens of 300 mm focal length. The beam is weakly focused and thus matched in size to the free-space interface in order to only illuminate the grating couplers on the ring-like layout. The beam waist of the focused Gaussian beam was ~250 µm, with the spot size of higher-order beams increasing accordingly[32,33]. The photonic processor is wire-bonded to a printed circuit board (PCB). The structured beam impinges normally onto the free-space interface where it couples to on-chip waveguide modes. The resulting on-chip light travels across the interferometric mesh and is processed by reconfiguring all interferometers while the transmitted on-chip intensities are recorded. In this experiment this is done off-chip by imaging the monitoring interface onto a conventional camera via a D-shaped pick-off mirror. Alternatively, power monitoring could be fully integrated on-chip, thus no longer requiring grating couplers. Both off-chip and on-chip power monitoring is discussed in more detail in the method section.

Now, we discuss what information the photonic processor can record in these measurements and what its advantages are compared to, e.g., a normal camera. Nowadays, structured higher-order beams can be generated with ease and their properties with

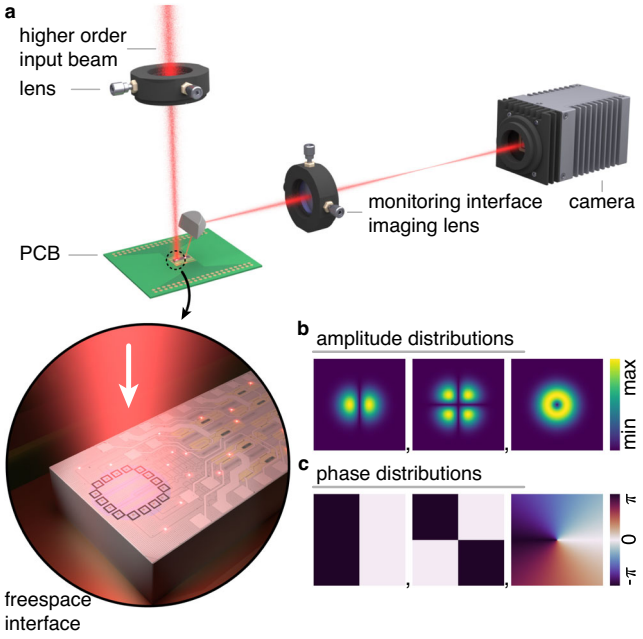

Fig. 2 Illustration of the experimental setup to measure higher-order beams. a Input beams are weakly focused onto the free-space interface of the photonic processor where they couple to on-chip waveguide modes which are processed on-chip in a mesh of interferometers while transmitted intensities are recorded off-chip by imaging the monitoring interface. **b**, **c** Ultimately, not only amplitude but also the phase information of the input beams is measured at each grating coupler position.

respect to intensity and phase distributions are well known theoretically. Experimentally, their intensity information can be accessed by, for example, placing a camera in the beam path of, e.g., a Laguerre-Gaussian beam $LG_{0,1}$, which reveals its ring-like intensity distribution. However, a camera is blind for the helical phase-front and the associated orbital angular momentum of such a beam. In contrast, our photonic processor is capable of measuring amplitude and phase distributions simultaneously, compare Fig. 2b, c respectively. In case of the Laguerre-Gaussian beam this can be used to immediately access the featured helical phase front and orbital angular momentum, as we will discuss in detail in the results section. Note that while this information is not directly accessible to conventional cameras, other techniques and devices, mentioned in the introduction, are able to access the phase information of, e.g., higher-order beams. Shack-Hartmann wavefront sensors with tens of thousands of pixels, for example,

can also measure phase information. Our multipurpose photonic processor is a powerful and versatile addition to the list of phase sensitive devices. Note, that the underlying principle of converting free-space light into on-chip waveguide modes, and vice versa, enables numerous novel applications across multiple research fields[13–17].

Phase and amplitude measurements. To demonstrate the capabilities of the integrated photonic processor in terms of measurements of higher-order beams and, where applicable, the identification of their orbital angular momentum, we measured different Hermite-Gaussian (HG)[34] and Laguerre-Gaussian (LG) beams[23]. In Fig. 3 we show the theoretical as well as measured amplitude and phase profiles of a Hermite-Gaussian beam $HG_{1,0}$, a $HG_{1,1}$ beam and a Laguerre-Gaussian beam $LG_{0,1}$. Theoretical distributions are plotted with high resolution in the background. Measured amplitude and phase values are superimposed as squares at the positions of the 16 individual grating couplers within the free-space interface of the photonic processor. To allow for a comparative analysis of relative amplitudes and to mitigate the impact of varying overall intensities, both the theoretical amplitude distributions and the measured amplitude values are normalized using their respective mean at the grating coupler positions. This normalization process ensures that both amplitude distributions center around a mean value of 1, and the relative variations in amplitude become qualitatively comparable. Theoretical expectation and experimental data are in very good agreement. In detail, the measured phases nicely follow both the abrupt phase changes of the Hermite-Gaussian beams and the gradually azimuthally changing phase in case of the Laguerre-Gaussian beam. For the latter, the phase clearly increases around the ring from 0 by 2π, corresponding to an orbital angular momentum of 1, i.e., the azimuthal index of the $LG_{0,1}$ beam. Minor deviations of the measured values could arise due to the intricate alignment of this few-pixels detector relative to the distributions of the light beam, modal imperfections of the input beams or minor systematic errors in the calibration, measurement or imaging of the photonic processor. These results showcase how our photonic processor can measure higher-order beams and provide insights into their amplitude and phase information.

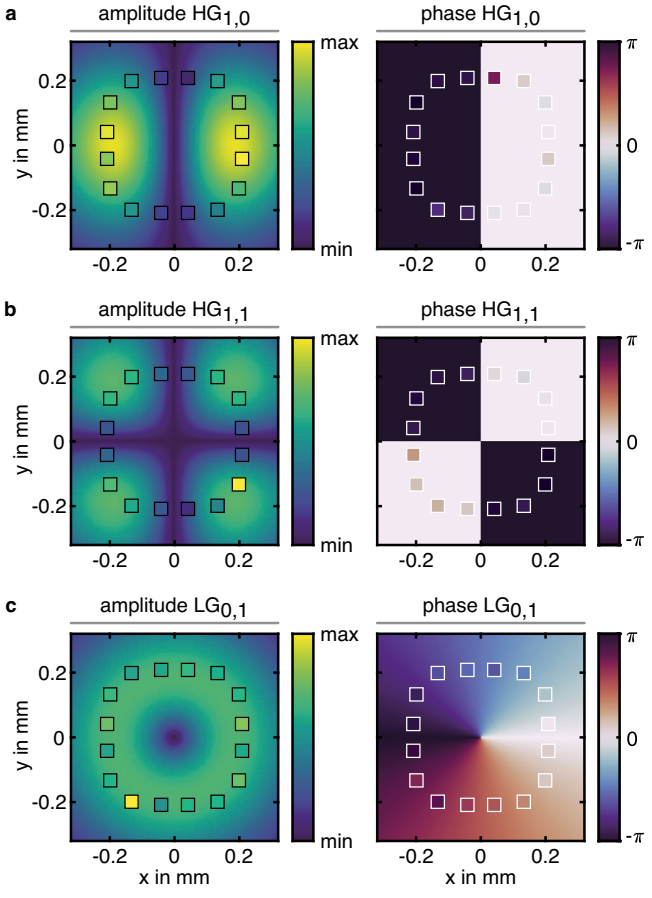

Fig. 3 Amplitude and phase distributions of higher-order spatial modes. Measured values are shown as squares at the 16 individual grating coupler positions. Theoretically calculated distributions are shown in the background. **a** Hermite-Gaussian beam $HG_{1,0}$. **b** Hermite-Gaussian beam $HG_{1,1}$. **c** Laguerre-Gaussian beam $LG_{0,1}$.

Distinction and identification of orbital angular momentum. While the detector's resolution with 16 pixels is limited, it allows for distinguishing the orbital angular momentum of input beams. The ring-like layout of the free-space interface does not resolve radial information with sufficient resolution, and we thus set the radial index of Laguerre-Gaussian input modes tested here to zero. We only measure azimuthal changes along the ring-like layout and thus change the index l of the input beams $LG_{0,l}$. This index is associated with the beam's orbital angular momentum. For a given $LG_{0,l}$ beam, the relative phases between neighboring pixels in the transverse plane increase or decrease linearly, depending on the sense of the spiraling phase-front of the beam. The overall phase change around the ring is $l \cdot 2\pi$. We show our experimental results of the measured phases for LG modes of azimuthal index 1 to 6 and -1 to -6 in Fig. 4(a) and (b), respectively. The measured phase values nicely follow the expected linear behavior with beams of higher azimuthal indices featuring a steeper slope. By fitting a linear regression to the measured data we can extract the individual slopes s of the curves and calculate the associated orbital angular momentum $l = 16s/2\pi$ of the various input beams. We include these linear fits in Fig. 4. The results of this orbital angular momentum retrieval method along with the resulting standard error are shown in Table 1. The retrieved orbital angular momentum values match the azimuthal index of the Laguerre-Gaussian input beams very well, both in case of positive and negative azimuthal indices. Deviations from the expected integer values of l are small and could arise from modal impurities of the input beam or other small systematic measurement errors. This shows that our photonic processor detects phases of higher-order beams very accurately and can be used to distinguish such beams based on phase information alone, which conventionally is difficult to access.

Conclusions

We have discussed and experimentally demonstrated the measurement of higher-order light beams using a multipurpose photonic integrated processor. Its free-space interface in combination with the on-chip light processing resolves amplitudes at the grating coupler positions while simultaneously also locally measuring relative phases. We showed the potential of such measurements by recording spatial amplitude and phase distributions of higher-order Hermite- and Laguerre-Gaussian beams and distinguishing Laguerre-Gaussian beams with azimuthal indices of up / down to ± 6. With only 16 pixels, this platform proves to be a powerful and versatile contender for characterizing orbital angular momentum and other free-space distributions of light. Recent advances related to programmable photonic processors could be readily implemented, extending the presented multipurpose photonic processor platform and directly improving its ability to measure amplitude and phase distributions. Larger and more generic input interfaces, polarization resolving grating couplers, the transition to visible wavelengths or

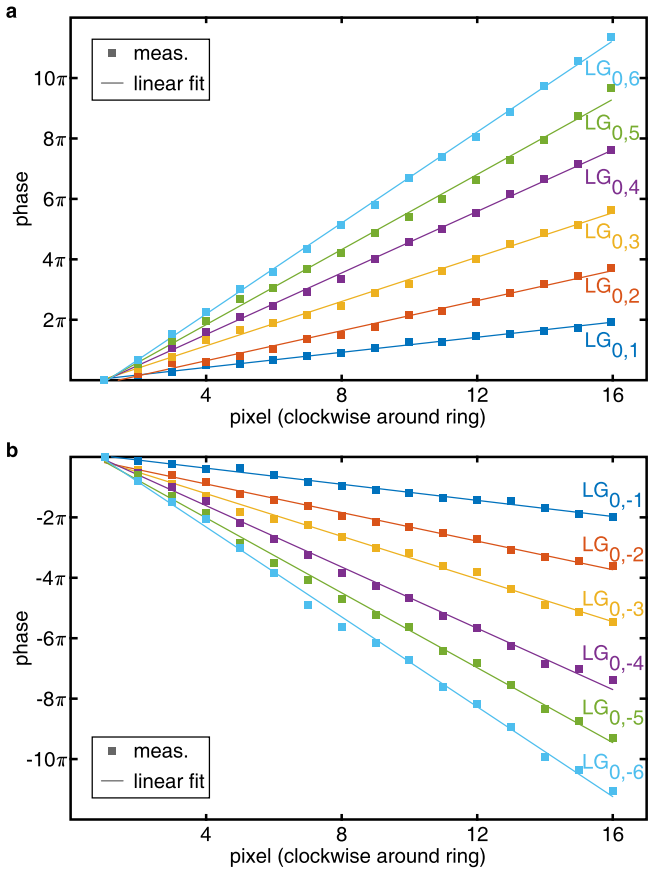

Fig. 4 Phase distributions of higher-order Laguerre-Gaussian beams. Measured phases (squares) of Laguerre-Gaussian beams of different azimuthal order. The phase is measured at the grating coupler / pixel positions numbered clockwise around the free-space interface. The phase increases linearly (fits shown as solid lines) and the overall change in phase around the ring varies by multiples of 2π. **a** Laguerre-Gaussian beams of azimuthal order 1 to 6. **b** Laguerre-Gaussian beams of azimuthal order -1 to -6.

Table 1 Measured orbital angular momentum and standard error of higher-order Laguerre-Gaussian input beams.

Beam	OAM_{meas}	Beam	OAM_{meas}
$LG_{0,1}$	1.00 ± 0.02	$LG_{0,-1}$	− 1.07 ± 0.03
$LG_{0,2}$	1.98 ± 0.04	$LG_{0,-2}$	− 1.89 ± 0.04
$LG_{0,3}$	2.93 ± 0.04	$LG_{0,-3}$	− 2.82 ± 0.05
$LG_{0,4}$	4.06 ± 0.04	$LG_{0,-4}$	− 4.06 ± 0.06
$LG_{0,5}$	4.96 ± 0.07	$LG_{0,-5}$	− 4.96 ± 0.07
$LG_{0,6}$	6.01 ± 0.04	$LG_{0,-6}$	− 5.95 ± 0.08

full integration of the monitoring interface are just a small selection of possible improvements. Already in its current form, the presented higher-order beam measurement of amplitude and phase as well as orbital angular momentum is a powerful tool and will find applications across various fields where, for instance, such knowledge gives deeper insights into the interaction processes light might have undergone with matter or the environment prior to detection.

Methods

Photonic circuit design. The reconfigurable photonic integrated circuit was fabricated commercially and is based on a 220 nm silicon-on-insulator platform. All waveguides in the photonic circuit are single-mode channel waveguides and have a width of 500 nm. Standard grating couplers, originally designed for fiber-coupling, where used to interface the photonic chip with free-space light. In total, they are ~16 µm wide by 40 µm long, have a grating pitch of 630 nm, and couple linearly polarized light (polarized along the direction of the grating grooves) to the transverse electric mode of the attached waveguides. They are designed for operation at 1550 nm, at which they emit light at an angle of ~12° to the surface normal of the chip. The free-space interface consists of 16 grating couplers, arranged along two concentric rings of 200 µm and 225 µm radii, with couplers oriented such that they are locally rotated by ± 45° with respect to the tangent line. Within the light processing unit, each on-chip interferometer is composed of two directional couplers (50:50 beam splitters), each with a length of 40 µm and a waveguide spacing of 300 nm. To reconfigure each interferometer, two TiN heaters (each 2 µm wide and 80 µm long) are placed above the waveguides, shifting the phase based on the thermo-optical effect. Thermal crosstalk is minimized by the implementation of thermal trenches which separate the TiN heaters from other waveguides in their close vicinity.

Power monitoring. After the light processing unit all waveguides are terminated by, again, grating couplers, in this case arranged along a line, spaced 127 µm apart. Imaging these on a conventional camera enables external power monitoring. The intensity of each grating coupler in the recorded image is directly proportional to the intensity of the on-chip waveguide mode. The imaging system is carefully designed with a combination of two 1-inch lenses of 100 mm focal length. These ensure a high imaging quality with low aberrations while still gathering all light emitted from the grating couplers. The use of a D-shaped pick-off mirror additionally improves the imaging quality. It blocks parts other than the free-space interface from being illuminated. Also, it prevents reflections from the photonic chip to hit the camera. Minor differences in the optical coupling at the different output gratings are not taken into account at this stage.

Alternatively, external power monitoring could be achieved by packaging a fiber array onto the output grating couplers and measuring the transmitted intensities with photodiodes. To realize an all-integrated version of the utilized system, power monitoring could also be fully integrated on-chip by using built-in photodiodes. Grating couplers in the monitoring interface would no longer be required. The integrated processor we utilize here even has built-in in-line power monitors[35], which can be seen in Fig. 1a on the right, between the central light processing unit and the grating couplers in the monitoring interface. However, these were not used for the presented experiments in order to reduce the systems' complexity.

Ring-like layout of the free-space interface. In the implemented free-space interface the local orientation of each grating coupler is dependent on its azimuthal position. As mentioned above, each grating coupler locally couples only linearly polarized light into the photonic circuit. While this could be utilized to also measure polarization distributions of light in the future, here we concentrate on amplitude and phase distributions only. Thus, in the present work, we always use circularly polarized input light to avoid any dependences on polarization. Note, that the azimuthally changing orientation of the grating couplers in the free-space interface combined with the circular input polarization results in an additional geometric phase, which we subtracted before displaying the data in this article.

This special layout of the free-space interface was specifically chosen to enable experiments that carry information mainly along the azimuthal direction, like the presented distinction of OAM of structured higher-order beams. However, the grating couplers sample (and emit) light of a specific wavelength predominantly under a specific angle (~12° at 1550 nm). Consequently, to ensure even coupling to all grating couplers with different local orientations, normal incidence is required. This shifts the wavelength at which the grating couplers operate most efficiently to longer wavelengths. To maintain a reasonable efficiency we adjust the wavelength of operation to 1570 nm. While the photonic circuit can still be calibrated and operated at this wavelength, operation at the design wavelength of the photonic components would be favorable. Experimentally, the need for normal incidence requires a thorough alignment with respect to the input light distribution. Misalignments are penalized by the resulting imbalance in the coupling efficiencies of the individual grating couplers. Additionally, at this stage, our few-pixel detector demands thorough alignment of the input light distribution with respect the position of the free-space interface. However, future generations of this device with more pixels (most likely in a grid like arrangement) will facilitate the detectors' usability. The focus will be more on the application than the layout of the free-space interface.

Operating the photonic integrated processor. In this work, the interferometric mesh is controlled and operated based on the approach described in Ref. [15]. The structured light sampled by the grating couplers of the free-space interface is processed on-chip by sequentially reconfiguring the interferometers in the central light processing unit. For every set of configurations of the interferometric mesh the power of all resulting/transmitted waveguide modes is being monitored. This set of measured intensities can next be matched via a least-squares fitting routine to a set of modeled intensities, calculated by describing the overall system theoretically. This theoretical description contains the transmission matrix of the interferometric mesh, which characterizes the on-chip processing of light and, among others, holds the configuration state of the mesh as free parameter. The theoretical description also contains the relative input waveguide amplitudes and phases.

Ultimately, knowing either two of these three quantities, (i) input light, (ii) mesh configuration, and (iii) transmitted light, allows the unknown third quantity to be reconstructed. Consequently, we first want to fully characterize the transmission matrix of the interferometric mesh (ii) in our experiment, which requires a calibration routine. By using a reference input, i.e., a single beam with a well-known phase front and a uniform amplitude distribution across all grating couplers, the relative input waveguide amplitudes and phases can be fixed in the theoretical description of the system. Recording a set of transmitted intensities for various configurations of the interferometric mesh and matching it to the modeled intensities then reveals all relevant parameters of the transmission matrix, thus calibrating this part of the system.

Next, with this information known, unknown input amplitudes and phases (i) can be subsequently sent onto the free-space interface. Recording and matching a set of transmitted intensities now reveals these input amplitude and phases at the grating coupler positions.

Lastly, we need to discuss how the photonic integrated processor is being controlled in order to record a sufficient set of transmitted intensities (iii). For this, we simultaneously scan all interferometers in the first column of the mesh, as indicated in Fig. 1b, through different configurations by applying a grid of 15-by-15 control voltages to the two integrated heaters of each respective interferometer. The transmitted intensities are being recorded. This is repeated sequentially for all four columns of the mesh. Control voltage values between 0.2 and 4 V where chosen to enable relative phase shifts between 0 and ~2π.

Regarding the speed of this approach to operation, at the present stage with no focus on this aspect each full measurement of relative input amplitude and phase takes ~2 min. However, the photonic processor can operate and adjust its individual configuration states at tens to hundreds of microseconds, before it is limited by the heat management in the interferometric mesh[13,16]. Future implementations could be dedicated to accelerate the operation, especially with faster, integrated and/or packaged power monitoring strategies implemented.

Data availability

Data underlying the results presented in this paper are not publicly available at this time but may be obtained from the authors upon reasonable request.

Received: 12 July 2023; Accepted: 30 November 2023;
Published online: 21 December 2023

References

1. Chen, X. et al. The emergence of silicon photonics as a flexible technology platform. *Proc. IEEE* **106**, 2101–2116 (2018).
2. Harris, N. C. et al. Linear programmable nanophotonic processors. *Optica* **5**, 1623 (2018).
3. Bogaerts, W. & Rahim, A. Programmable photonics: an opportunity for an accessible large-volume pic ecosystem. *IEEE J. Select. Topics Quant. Electron.* **26**, 1–17 (2020).
4. Bogaerts, W. et al. Programmable photonic circuits. *Nature* **586**, 207–216 (2020).
5. Annoni, A. et al. Unscrambling light-automatically undoing strong mixing between modes. *Light Sci. Appl.* **6**, e17110 (2017).
6. Carolan, J. et al. Universal linear optics. *Science* **349**, 711–716 (2015).
7. Pérez, D. et al. Multipurpose silicon photonics signal processor core. *Nat. commun.* **8**, 636 (2017).
8. Shen, Y. et al. Deep learning with coherent nanophotonic circuits. *Nat. Photon.* **11**, 441–446 (2017).
9. Pai, S. et al. Experimentally realized in situ backpropagation for deep learning in photonic neural networks. *Science* **380**, 398–404 (2023).
10. Pai, S. et al. Experimental evaluation of digitally verifiable photonic computing for blockchain and cryptocurrency. *Optica* **10**, 552 (2023).
11. Miller, D. A. B. Self-configuring universal linear optical component. *Photon. Res.* **1**, 1 (2013).
12. Miller, D. A. B. Self-aligning universal beam coupler. *Opt. Expr.* **21**, 6360–6370 (2013).
13. Bütow, J., Eismann, J. S., Sharma, V., Brandmüller, D. & Banzer, P. Generating free-space structured light with programmable integrated photonics. *arXiv* https://arxiv.org/abs/2304.08963 (2023).
14. Miller, D. A. B. Analyzing and generating multimode optical fields using self-configuring networks. *Optica* **7**, 794 (2020).
15. Bütow, J. et al. Spatially resolving amplitude and phase of light with a reconfigurable photonic integrated circuit. *Optica* **9**, 939 (2022).
16. Milanizadeh, M. et al. Separating arbitrary free-space beams with an integrated photonic processor. *Light Sci. Appl.* **11**, 197 (2022).
17. Milanizadeh, M. et al. Coherent self-control of free-space optical beams with integrated silicon photonic meshes. *Photon. Res.* **9**, 2196 (2021).
18. Mair, A., Vaziri, A., Weihs, G. & Zeilinger, A. Entanglement of the orbital angular momentum states of photons. *Nature* **412**, 313–316 (2001).
19. Hell, S. W. Far-field optical nanoscopy. *Science* **316**, 1153–1158 (2007).
20. Willner, A. E. et al. Optical communications using orbital angular momentum beams. *Adv. Opt. Photon.* **7**, 66 (2015).
21. Rubinsztein-Dunlop, H. et al. Roadmap on structured light. *J. Opt.* **19**, 013001 (2017).
22. Willner, A. E., Pang, K., Song, H., Zou, K. & Zhou, H. Orbital angular momentum of light for communications. *Appl. Phys. Rev.* **8**, 041312 (2021).
23. Allen, L., Beijersbergen, M. W., Spreeuw, R. J. & Woerdman, J. P. Orbital angular momentum of light and the transformation of laguerre-gaussian laser modes. *Phys. Rev. A* **45**, 8185–8189 (1992).
24. Fatkhiev, D. M. et al. Recent advances in generation and detection of orbital angular momentum optical beams-a review. *Sensors* **21**, e50028 (2021).

25. Berkhout, G. C. G., Lavery, M. P. J., Courtial, J., Beijersbergen, M. W. & Padgett, M. J. Efficient sorting of orbital angular momentum states of light. *Phys. Rev. lett.* **105**, 153601 (2010).
26. Forbes, A., Dudley, A. & McLaren, M. Creation and detection of optical modes with spatial light modulators. *Adv. Opt. Photon.***8**, 200 (2016).
27. Sharifi, S., Banadaki, Y., Veronis, G. & Dowling, J. P. Towards classification of experimental laguerre–gaussian modes using convolutional neural networks. *Opt. Eng.* **59**, 1 (2020).
28. Rui, G., Gu, B., Cui, Y. & Zhan, Q. Detection of orbital angular momentum using a photonic integrated circuit. *Sci. Rep.* **6**, 28262 (2016).
29. Chen, J., Chen, X., Li, T. & Zhu, S. On-chip detection of orbital angular momentum beam by plasmonic nanogratings. *Laser Photon. Rev.* **12**, 1700331 (2018).
30. Sun, J., Timurdogan, E., Yaacobi, A., Hosseini, E. S. & Watts, M. R. Large-scale nanophotonic phased array. *Nature* **493**, 195–199 (2013).
31. Heck, M. J. Highly integrated optical phased arrays: photonic integrated circuits for optical beam shaping and beam steering. *Nanophotonics* **6**, 93–107 (2017).
32. Carter, W. H. Spot size and divergence for hermite gaussian beams of any order. *Appl. Opt.* **19**, 1027–1029 (1980).
33. Phillips, R. L. & Andrews, L. C. Spot size and divergence for laguerre gaussian beams of any order. *Appl. Opt.* **22**, 643–644 (1983).
34. Svelto, O. *Principles of Lasers* 5th edn, Vol. 2 (Springer New York, 2010).
35. Morichetti, F. et al. Non-invasive on-chip light observation by contactless waveguide conductivity monitoring. *IEEE J. Select. Topics Quant. Electron.* **20**, 292–301 (2014).

Acknowledgements

This work was supported by the European Commission through the H2020 project SuperPixels (grant 829116). The financial support by the Austrian Federal Ministry of Labor and Economy, the National Foundation for Research, Technology and Development and the Christian Doppler Research Association is gratefully acknowledged. The authors acknowledge the financial support by the University of Graz. The authors thank all members of the SuperPixels consortium for fruitful discussions and collaboration. We thank Maziyar Milanizadeh, Francesco Morichetti, Charalambos Klitis, and Marc Sorel for the photonic circuit design.

Author contributions

P.B., J.S.E., V.S. and J.B. conceived the idea. V.S. and D.B. performed the experiment. V.S. and J.B. analyzed the data. V.S., J.B. and P.B. wrote the manuscript. P.B. supervised the project.

Competing interests

The authors declare no competing interests.

Additional information

Correspondence and requests for materials should be addressed to Peter Banzer.

Peer review information *Communications Physics* thanks Vijay Kumar, Sha Zhu and the other, anonymous, reviewer(s) for their contribution to the peer review of this work.

Reprints and permission information is available at http://www.nature.com/reprints

Publisher's note Springer Nature remains neutral with regard to jurisdictional claims in published maps and institutional affiliations.